Co-pyrolysis of beech wood and polyamide-6: Impact of plastic concentration and wood/plastic synergistic effects

William de Rezende Locatel, Chetna Mohabeer, Dorothée Laurenti, Yves Schuurman, Nolven Guilhaume

Co-pyrolysis of beech wood and polyamide-6 : Impact of plastic concentration and wood/plastic synergistic effects

William de Rezende Locatel, Chetna Mohabeer, Dorothée Laurenti, Yves Schuurman, Nolven Guilhaume*

Univ. Lyon, Université Claude Bernard Lyon 1, CNRS, IRCELYON – UMR 5256, 2 Avenue Albert Einstein, F-69626 Villeurbanne Cedex, France

* Corresponding author, nolven.guilhaume@ircelyon.univ-lyon1.fr

Abstract

Biomass residues and waste can be converted into bioliquids by pyrolysis, which can contribute to both the production of renewable fuels and the recycling of waste. In this paper, the catalytic co-pyrolysis of mixtures of beech wood (BW) and polyamide-6 (PA6) in different ratios was investigated to assess the effect of PA6 concentration on the properties of bio-oils and on the catalyst performances in upgrading the bio-oils. The catalytic treatment was applied to the pyrolysis vapors that were driven across a H-ZSM-5 catalyst bed before their condensation into liquid products. Increasing the PA6 concentration in the BW+PA6 blends led to an increase in the average molar mass of bio-oils and to an increase in their N-content. Caprolactam and 5-cyano-1-pentene were the main products derived from PA6 pyrolysis, and their ratio also changed with the PA6 concentration. The production of fully deoxygenated compounds was strongly reduced in the presence of PA6, as the result of catalyst deactivation, also evidenced by the increase in sugars and decrease in furans concentrations. The amount of coke deposited on the catalyst decreased as the PA6 concentration increased, but this coke contained more nitrogen. Synergistic effects in the BW+PA6 pyrolysis were evidenced by the positive or negative deviation of different parameters (mass of gas, liquid, solid products, mass of coke on the catalyst, C, N, O composition of bio-oils) from a simple arithmetic combination of the same parameters for pure BW or pure PA6 weighted by their concentrations, in particular the N-content in the bio-oils was much higher than expected.

Keywords: Biomass pyrolysis; polyamide pyrolysis; co-pyrolysis; Bio-oils; Catalytic upgrading.

1. Introduction

Co-pyrolysis of wood and plastics could be considered in the near future to recycle waste biomass, in particular municipal waste and construction wood, which generally also contain plastics. Among these plastics, N- or Cl-containing plastics such as polyamide or polyvinylchloride have been little studied and should also be considered, given their wide use in many applications, but also because waste biomass contains various types of plastics that cannot be easily sorted and separated according to their composition. In a previous study [1], the co-pyrolysis of beech wood (BW) and polyamide-6 (PA6) chips was investigated and the effect of ex-situ treatment of the pyrolysis vapors using a HZSM-5 catalyst was assessed. However, the biomass/plastic ratio is also an important parameter that affects the pyrolysis process and the products quality [2], through interactions between the wood chips and the plastic particles, or among their degradation products, that can lead to synergistic effects.

Most of the studies dealing with synergistic effects in co-pyrolysis were carried out using polyolefin-based polymers like PP and PE, or polyaromatics like PS, which do not contain heteroatoms (Cl, N) that could affect the pyrolysis process and impair the catalyst performances, when a catalytic treatment is applied. For instance, aiming to identify the mechanisms responsible for this synergistic effect, Cheng and Huber [3] studied the conversion of furanic compounds (furan, 2-methylfuran, furfural, and furfuryl alcohol) and olefins (ethylene and propylene) over ZSM-5 in a fixed-bed reactor operating between 450°C and 600°C. An increase in aromatics selectivity was observed when propylene was added to the feed, due to the occurrence of Diels-Alder reactions. The authors also reported that furfural and furfuryl alcohol underwent decarbonylation to produce furan and CO. Finally, a decrease in coke and CO_2 yields was observed, suggesting that the presence of hydrogen-rich reactants such as olefins modified the reaction pathways for oxygen removal, shifting from decarbonylation and decarboxylation to dehydration.

Liu and coworkers [4] also evaluated the synergistic effects observed during co-pyrolysis of pinewood and polypropylene carried out without a catalyst in a fixed-bed reactor at 900°C. The authors reported an increase in syngas (H_2 and CO) production and a decrease in the formation of non-condensable hydrocarbons and in chars. These effects were assigned to the interaction between oxygen-containing radicals in the volatiles evolved from pinewood with hydrogen-rich

radicals from the polymer that act as H-donor species, which promoted pinewood volatilization and inhibited the condensation and repolymerization reactions, hence reducing the char formation.

Li et al.[5] studied the catalytic fast pyrolysis (CFP) of cellulose and low-density polyethylene (LDPE), polypropylene (PP) and polystyrene (PS) employing HZSM-5 as catalyst. Among the plastics studied, LPDE showed a higher synergistic effect, with a significant increase in aromatic yield and a reduction in coke formation. These effects were ascribed to interactions between volatiles from plastic and biomass, as discussed previously. However, when the reaction was performed with PP, the synergistic effect was smaller than that observed with LDPE. The explanation relies on the higher concentration of branched olefins obtained with PP when compared to LDPE. The electronic phenomena and steric hindrance of their branching prevented the Diels-Alder reactions essential to the formation of aromatic compounds. Finally, the co-pyrolysis with PS showed the lowest synergistic effect, with insignificant interactions between PS and cellulose; however, an increase in aromatics yield was observed, mainly due to the aromatic nature of PS itself that depolymerizes into styrene and polyaromatic species.

Ghorbannezhad et al.[6] evaluated the co-pyrolysis of sugarcane bagasse pith and polyethylene terephthalate (PET) in a tandem micro-reactor at 700 °C using HZSM-5 and sodium carbonate/γ-alumina as catalysts. The main results were an increase in aromatics formation (especially benzene, toluene, xylene, and ethylbenzene - BTXE) and a reduction in coke deposition in the presence of the plastic. The hypothesis proposed for these observations was the occurrence of H-transfer from PET-derived aliphatics towards lignin-derived oxygenated compounds, contributing to the hydrocarbon pool pathway and avoiding cross-linking reactions that result in char formation. However, the decomposition of PET also resulted in the formation of benzoic acid, which is detrimental to bio-oil quality [7].

As our current situation stands, the concentrations of polyamide-based plastics in municipal solid waste (MSW) are expected to increase in the next years due to the COVID-19 pandemic and the massive utilization of personal protective equipment, notably disposable masks that are made from woven polyamide tissues. Therefore, this study focuses on co-pyrolysis of beech wood (BW) and polyamide-6 (PA6) at concentrations between 5 and 20 wt.% (close to those found in municipal solid waste [8, 9], aiming at understanding the synergistic effects between them and the chemical processes involved. All co-pyrolysis experiments were carried out using HZSM-5 as

catalyst for ex-situ treatment of the pyrolysis vapors. In combination with a previous publication on this topic [1] that assessed more specifically the role of the HZSM-5 catalyst, the present study covers the most important aspects related to the co-pyrolysis of lignocellulosic biomass and polyamide, which are scarce in the literature. In addition, this work presents an extensive range of characterizations of the liquid, gaseous and solid products obtained by co-pyrolysis, as well as the characterization of fresh and spent catalysts.

2. Experimental section

2.1. Feedstocks

The lignocellulosic biomass used consists of beech wood chips supplied by J. Rettenmaier & Söhne; they were sieved to obtain particle sizes I, the range from 0.75 to 1.7 mm. Polyamide-6 (BASF - Ultramid® B) was supplied as pellets, which were crushed and sieved before use to obtain particle sizes in the same range as the wood chips. BW chips were mechanically mixed with 5, 10 and 20 wt.% of PA6 (on dry basis). All feedstock samples were dried in an oven at 110°C for 1h before each pyrolysis experiment and stored in airtight flasks.

2.2. Catalyst

Zeolite HZSM-5 with a molar Si/Al ratio of 40 was supplied by Céramiques Techniques Industrielles (CTI) Salindres, France. The catalyst characterization has been described previously [10] and its main properties are summarized in Table 1.

Table 1 - Properties of HZSM-5 catalyst

Property	**Value**
Particle size (µm)	100-300
Water content[a] (% wt.)	3.9
Si/Al atomic ratio[b] (SAR)	40.5
Total SSA[c] (m^2g^{-1})	423
Microporous surface (m^2g^{-1})	363
External surface (m^2g^{-1})	60
Average pore diameter[d] (nm)	0.55

Total pore volume (cm^3g^{-1})	0.18
Brønsted acid sites [e] (µmol/g)	127
Lewis acid sites [e] (µmol/g)	45

[a] measured by TGA; [b] measured by ICP; [c] BET method; [d] from International Zeolite Association database; [e] measured by FT-IR of pyridine adsorbed at 150°C.

2.3. Pyrolysis set-up

Co-pyrolysis of beech wood and PA6 was carried-out in a lab-scale pyrolytic bench already described [11], with a few modifications to adapt the system to the mixed wood/plastic feedstocks (Figure 1). The jacketed reactor has an internal zone where the thermal pyrolysis is carried out and a bed of catalyst can be placed (or not) just below to treat the vapors which come out of the pyrolysis zone. The BW chips or BW+PA6 blends were previously dried at 110°C for 1.5 h before being placed in the gas-tight hopper and kept under N_2 atmosphere.

Unlike the previous description [11], the new inner reactor (pyrolysis zone) was a straight quartz tube, in which the solid chips were fed semi-continuously from the top for 1 h, by small increments of ≈0.045 g every 10 s, and fell down by gravity onto a quartz porous frit at the bottom of this section, where the chars and solid residues were retained. The total mass of solid chips fed in the reactor was ≈16 g in 1 h of experiment. The temperature in the pyrolysis zone was 450-500°C along the tube and 480°C on the porous frit where the wood chips were stopped. The pyrolysis vapors (formed by thermal pyrolysis) were entrained downstream by a nitrogen flow of 260 smL/min (flow rate standardized at 0°C and 1 atm) and passed through the catalyst bed placed just below the pyrolysis zone on a second quartz frit. All pyrolysis experiments were carried out with *ex-situ* catalytic treatment of the vapors using the HZSM-5 catalyst described previously. The temperature of the catalyst bed was 453 ± 2°C. In this external part of the reactor, an additional gas flow composed of 240 smL/min N_2 and 20 smL/min He (used as internal standard for GC analysis) was added to prevent retro-diffusion of the vapors and to adjust the total gas flow rate. The residence time of the vapors in the pyrolysis zone was estimated at 41 s, while the contact time with the catalyst (when present) was around 2 s. The pressure in the reactor was continuously monitored by a pressure sensor connected to a safety device which cuts off the experiment automatically if the pressure exceeds 1.3 bars. The pressure measured during the experiments was around 1.1 bar.

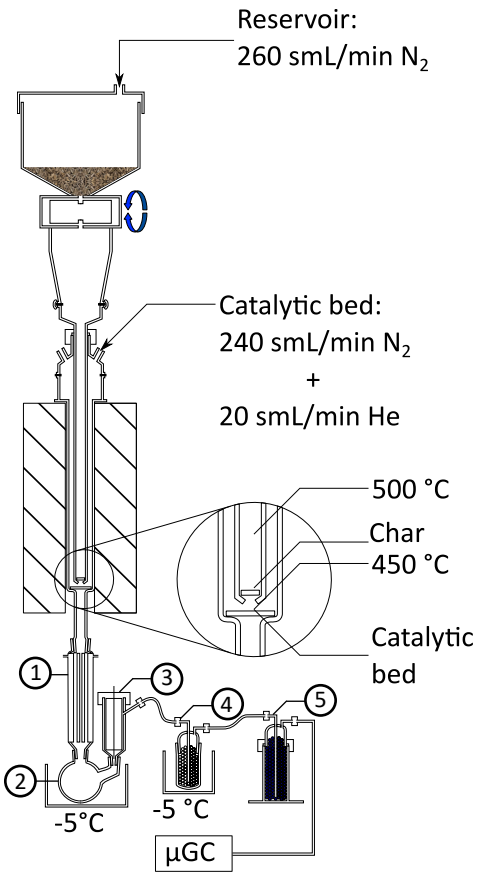

Figure 1 - Pyrolysis setup scheme

The vapors were condensed downstream the reactor and collected in a series of traps including a condenser (1) and a round bottom flask (2) both cooled at -5°C, an electrostatic precipitator (3), a trap filled with glass beads at -5°C (4) and a trap at ambient temperature filled with silica gel beads (5), that prevented any condensable compound from being introduced in the micro-GC for online gas phase analysis. The total mass of bio-oils formed in the experiments was assessed by mass difference, by weighing the different glassware parts before and after the experiments.

Prior to starting the reaction, the reactor was loaded with 2 g of catalyst and heated to 500 °C under a N_2 flow for 2 h to ensure fully stabilized temperatures in the whole system (reactor and cold traps) and to desorb the water adsorbed on the catalyst.

2.4. Products recovery

Non-condensable gaseous products (hereinafter called "gas phase") were analyzed and quantified online using a micro-GC.

The fractions called "aqueous phase" and "organic phase" were recovered directly in the round bottom flask and simply separated by centrifugation; thus, they constituted the most representative share of the bio-oil produced in the process. Other fractions of bio-oils were also deposited in the downstream traps and remained stuck on the glassware parts. In order to obtain a detailed mass balance, these fractions were recovered by washing the glassware with methanol, followed by evaporation of the methanol at 50°C under a pressure of 400 mbar, yielding the "recovered organic phase". However, the evaporation step was found to modify the composition of this bio-oil fraction due to simultaneous evaporation of volatile components. In addition, ^{13}C-NMR analysis showed the presence of residual methanol in this fraction. Therefore, it was decided not to mix the "recovered organic phase" with the native "organic phase". Finally, a part of the bio-oil could not be recovered because it was adsorbed on the silicagel beads or lost during the different steps of recovering the other fractions. This fraction was called "organic not recovered" and was quantified by weighing the glassware parts before and after experiment.

The chars were recovered from the first quartz frit, weighed and are hereinafter called "solid phase".

2.5. Product characterization

Gaseous products were analyzed online using a micro gas chromatograph Inficon 3000 (SRA instruments) equipped with three analytical modules and TCD detectors, calibrated with appropriate compound mixtures. A MolSieve column equipped with a Plot U pre-column was used to analyze He, H_2 and CO; a Plot U column was used to analyze CO_2, C_2H_4 and C_2H_6; an alumina column was used to analyze the remaining hydrocarbons (C_3-C_5). The duration of each analysis was 6 minutes and the analyses were repeated over 90 minutes. Helium was used as internal standard to account for the variations of total gas flow rates at the reactor inlet and outlet.

Elemental compositions (CHNS) were obtained with a Flash2000 (Thermo Scientific) equipment. For each analysis, a known mass of sample (1-3 mg) was placed in a tin crucible and each measurement was repeated three times to determine the measurement uncertainty.

The HHV was calculated from the elemental analysis using the equation proposed by Channiwala and Parikh [12].

$$\mathrm{HHV} = 0.3491[\mathrm{C}] + 1.1783[\mathrm{H}] - 0.1034[\mathrm{O}] - 0.0151[\mathrm{N}]$$

In this equation the HHV is expressed in MJ/kg and [C], [H], [N] and [O] in mass percentages on dry basis.

The water content of bio-oils was determined by Karl-Fischer (KF) titration using a Metrohm Titrando 852 analyzer. The samples were diluted in THF at a concentration of 10 wt.% and the volumetric method was employed. To avoid side reactions of aldehydes and ketones with traditional KF reagents, which produce water, specific reagents for samples containing these organic compounds were chosen: Karl Fischer ROTI hydroquant C5K (5 mg of water/mL of solution) and Karl Fischer ROTI hydroquant working medium K. The calibration was carried out using a solution of 10 wt.% of H_2O in THF.

Molar mass distributions were obtained by gel permeation chromatography (GPC) using an Agilent equipment (1200 series) equipped with two PL gel columns with different pore sizes (500 and 50 Å) using THF as the mobile phase (1 mL/min). Two detectors were used, a refractive index detector (RID) and diode-array detector (DAD), collecting data each 0.4 s in the range of 200-450 nm with a resolution of 2 nm. The samples were prepared with concentration of 1 wt.% in THF and filtered before analysis (PTFE – 0.45μm). The measurements were carried out at 35°C and the calibration was performed using hydrocarbons standards (molecular weight between 86 and 1000 g/mol).

^{13}C nuclear magnetic resonance (^{13}C-NMR) spectra were recorded using a Bruker AVANCE 400 MHz spectrometer and the spectra were analyzed with the TopSpin 3.0 software. The analyses were carried out at room temperature with an accumulation of 4500 scans. Trioxane was used as internal standard, diluted in DMSO-D6 in a coaxial tube configuration that prevented the contact of the solvent with the bio-oil samples.

Gas chromatography coupled with a mass spectrometer was performed with a GCMS-QP2010 SE apparatus (Shimadzu) equipped with a Zebron ZB Wax-Plus column (length 60 m, internal diameter 0.25 mm, film thickness 0.25 μm). The samples were diluted in methanol (20 wt.% for organic phase and 30 wt.% for aqueous phase) and filtered before the analysis (Cellulose acetate

208 – 0.45µm). The oven temperature program started at 70 °C (held for 10 min), then was heated at a
209 rate of 5°C/min up to 150 °C. At this point the heating rate changed to 3°C/min up to 250 °C (held
210 for 15 min).

211 Two-dimensional gas chromatography coupled with mass spectrometry (GCxGC-MS) was
212 carried out with an Agilent GC 6890N apparatus. The first separation was performed by a polar
213 column VF-1701 MS (I.D 0.25 mm; film thickness 0.25 µm; length 30 m) followed by a second
214 apolar column DB1 (I.D 0.25 mm; film thickness 0.25µm; length 1.5m) for the second dimension
215 of separation. The modulation was performed by a cryogenic modulator (Zoex Corporation USA)
216 each 12s. The compounds were identified by the coupled MS detector (5975B). The use of a first
217 polar column followed by a less polar column favored the separation of oxygen and nitrogen-
218 containing compounds, widely present in bio-oils [13]. The temperature program was set as
219 follows: first column from at 50°C to 300 °C with a ramp of 1.75 °C/min, then to 320°C with a
220 ramp of 1.8 °C/min. The second column went from 50 °C to 320°C at 1.8 °C/min. The samples
221 concentration was the same as described for GC-MS analyses.

222 The spent catalyst (recovered after reaction) was analyzed by thermogravimetric analysis
223 (TGA) under air (40 mL/min) using a TGA/DSC-1- Star^e system (Mettler Toledo) equipped with
224 a gas controller GC200. The temperature was initially held at 25°C for 5 minutes, then increased
225 up to 900°C with a heat-up ramp of 10°C/min.

226

227 **3. Results and discussion**

228 **3.1. Co-pyrolysis of BW and PA6 and products characterization**

229 The selectivity for gas, liquid and solid products is displayed in Figure 2. The mass balance
230 obtained for all reactions was ≥ 95% and generally close to 100%, and the liquid products were
231 the main fraction collected, including when pure PA6 was used.

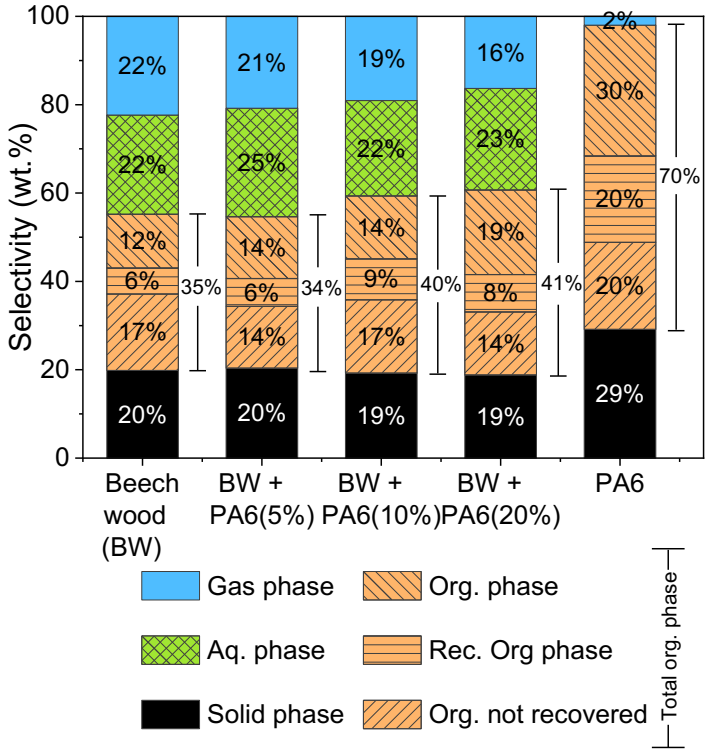

Figure 2 - Product selectivity in experiments with different concentrations of PA6

The increase in PA6 concentration led to a decrease in the production of gaseous products associated with an increase in the selectivity in liquid products, essentially the organic phase. With pure PA6 there was no phase separation of the liquid fraction, which consists only of an organic phase. Since PA6 does not contain any water or hydroxyl groups its degradation is less likely to yield water than that of biomass. PA6 also yielded more solid products than BW+PA6 blends, but the solid residues included a significant part of white polymer particles, collected downstream the reactor, probably formed by re-condensation of PA6-derived monomers or oligomers.

Figure 3 shows the cumulative production of all non-condensable products, normalized by unit mass of feedstock. Increasing the concentration of PA6 in BW+PA6 blends led to a decrease in the production of gases, and the pyrolysis of pure PA6 produced the fewest gaseous products, indicating that, unlike wood, PA6 and its pyrolysis products cracked only marginally into light compounds.

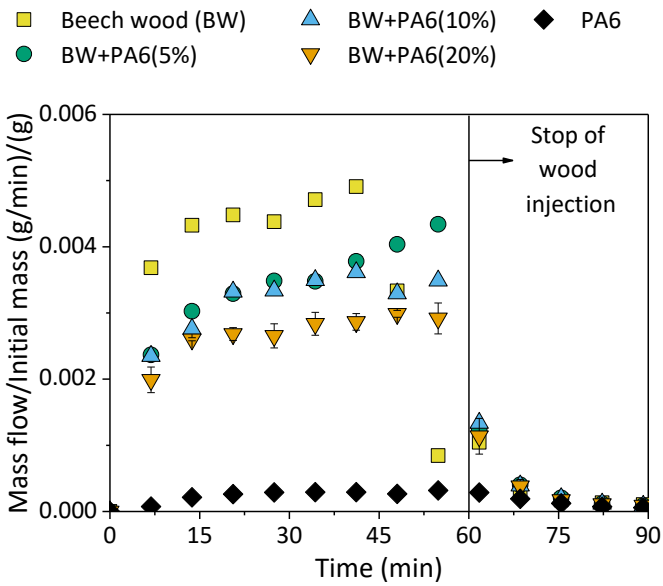

Figure 3 - Total mass flow of gaseous products normalized by the initial mass of feedstock

The composition of the gas phase is detailed in Figure 4. The increase in plastic concentration led to a decrease in CO_x and C_2-C_3 olefins production, and to a small but significant increase in light paraffins production ($C_{2\text{-}6}^{paraf}$), while less olefins (ethylene and propene) are formed. The changes in CH_4 and H_2 production from BW and BW+PA6 were statistically insignificant, but pure PA6 produced almost no methane or hydrogen, which suggests that they are essentially produced from the wood. Finally, H_2 was a minor product in all experiments in terms of mass, but also in terms of moles.

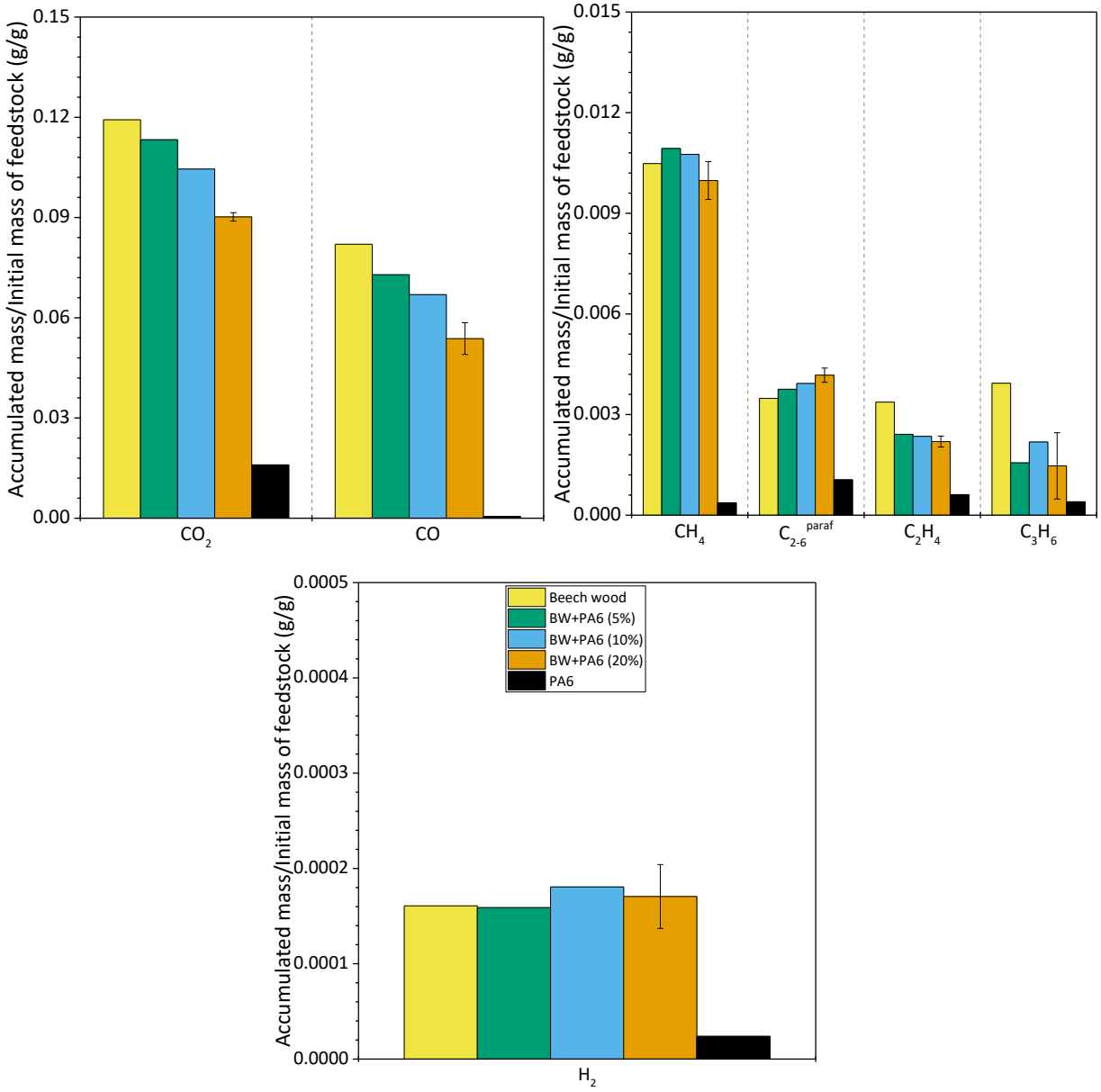

Figure 4 - Cumulative mass of non-condensable gases, normalized by unit mass of feedstock

Table 2 shows the water content, the ultimate analysis and the calculated higher heating value (HHV) of the two liquid phases obtained in the experiments. The CHNO analyses were calculated on dry basis, therefore they represent the composition of what is not water, in both types of liquid phases.

Table 2 - Water content, ultimate analysis and HHV of the liquid fractions.

Feedstock	%H_2O	Ultimate analysis (wt.% on dry basis)				HHV (MJ/kg)
		C	H	N	O*	
Organic phase						
Beech wood	11.9±1.8	70.6±1.2	6.4±0.6	0.5±0.6	22.4±0.6	29.9±0.8
BW+PA6 (5%)	12.5±1.1	68.3±1.3	7.0±0.3	2.4±0.8	22.3±1.7	29.8±0.2
BW+PA6 (10%)	13.4±0.8	70.5±0.3	7.11±0.02	3.8±0.7	18.6±1.0	31.0±0.2
BW+PA6 (20%)	13.8±1.4	71.6±2.4	7.5±0.5	6.1±0.4	14.8±2.2	32.2±0.7
PA6	15.2±1.0	74.8±0.7	9.7±0.1	14.3±0.2	1.2±0.5	37.2±0.2
Aqueous phase						
Beech wood	78.9±1.3	61.3±1.6	3.9±3.2	2.1±1.3	32.7±2.2	23.5±2.6
BW+PA6 (5%)	74.3±0.7	62.0±3.3	6.2±0.4	3.6±0.7	28.2±2.9	26.0±1.9
BW+PA6 (10%)	76.2±6.2	66.4±2.5	4.6±1.6	5.8±2.2	23.3±5.0	26.1±2.7
BW+PA6 (20%)	65.8±2.3	54.5±1.8	6.2±7.2	8.7±1.8	30.6±5.3	23.1±8.9

* by difference.

The increase in PA6 concentration resulted in an increase in the water content in the organic phase, and to the opposite in the aqueous phase (not present with pure PA6). This could be related to the fact that caprolactam, which is the main product of PA6 degradation as will be shown later, is hygroscopic [14]: when the content of PA6 increased, there was more caprolactam in the organic phase, which could promote water solubility in this phase. The organic phase obtained from pure BW contained ≈0.5 wt.% N and the aqueous phase ≈2 wt.%. Using BW/PA6 blends, the N-content in both phases increased regularly with PA6 concentration, which suggests that N-containing compounds derived from PA6 are shared out in both organic and aqueous phases. PA6 also contains oxygen in the form of a carbonyl group and oxygen accounts for ≈14 wt.% of its molar mass, while beech wood contains ≈44 wt.% O. Therefore, the oxygen content in the liquid fractions originated predominantly from the biomass. Accordingly, reducing the BW fraction in the

feedstock led to a lower oxygen content in the organic phase (Table 2), the HHV increased with the percentage of PA6 and the organic phase obtained from pure PA6 showed the highest HHV.

A number of studies reviewed by Ansari et al. [15] reported that the co-pyrolysis of biomass with various types of plastics results in bio-oils with higher H/C ratios, the plastic behaving as hydrogen-donor for intermolecular H-transfer. In the present study, the Van Krevelen diagram (Figure 5) indeed showed a slight increase in the H/C ratio for organic phases produced from BW+PA6 blends, but the difference was within the margin of error.

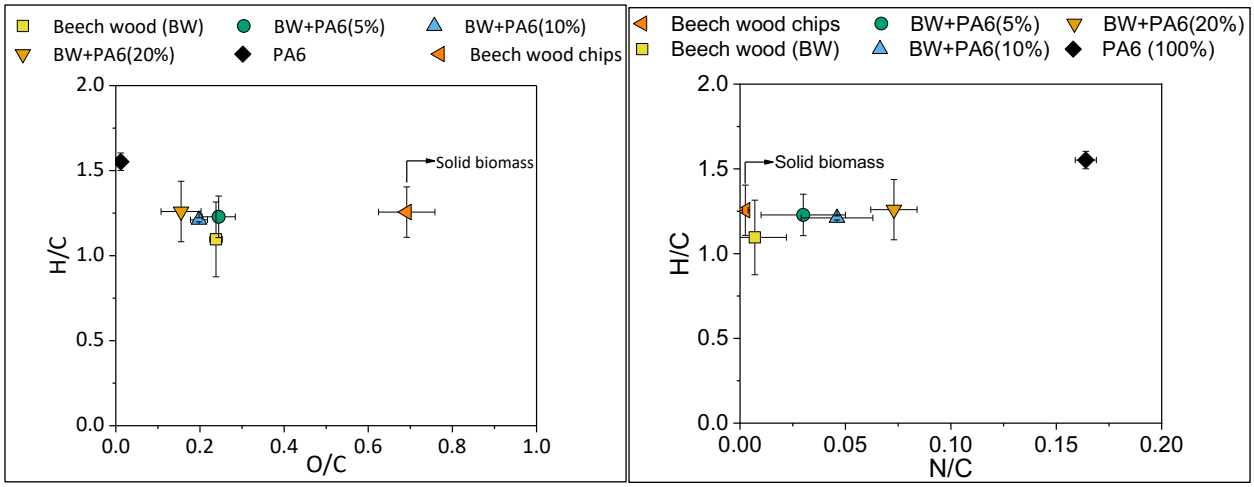

Figure 5 - Van Krevelen diagrams of liquid organic phases compared to solid beech wood

The N/C ratio increased strongly with PA6 concentration, but this increase was not proportional to the concentration of PA6 in the BW+PA6 blends. This trend will be discussed in paragraph 3.3.

Figure 6 specifically shows the distribution of N-containing compounds identified by GC-MS in both organic and aqueous phases. The percentages are expressed relative to the total peaks area.

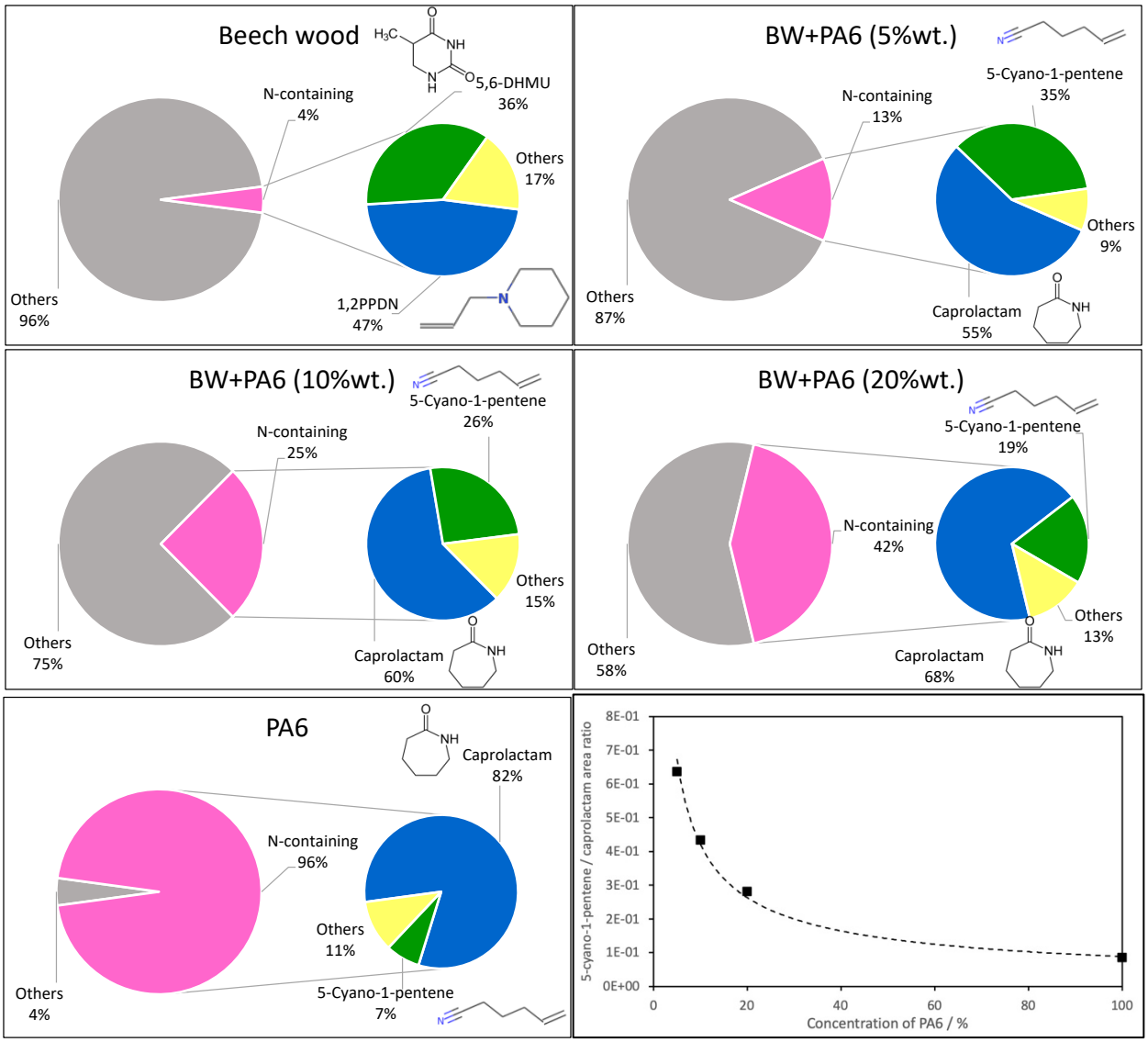

Figure 6 - N-containing products distribution in the organic phases and 5-cyano-1-pentene/caprolactam ratio as a function of PA6 concentration

For experiments with pure BW, 4% of the total peaks area corresponded to N-containing compounds. This fraction consisted mainly of 1-(2-propenyl)piperidine (1,2PPDN – 47%) and 5,6-dihydro-5-methyluracil (5,6-DHMU – 36%). These compounds are related to biological functions and metabolic processes in biomass. Adding 5 wt.% of PA6 to BW led to 13 % of N-containing compounds (relative to the total peaks area), and within these 55% was caprolactam, 35% 5-cyano-1-pentene and the remaining 9% other N-containing compounds. The complete list of analyzed compounds can be found in the supplementary information.

In all experiments in the presence of PA6, the main N-products were caprolactam and 5-cyano-1-pentene. However, the 5-cyano-1-pentene/caprolactam ratio decreased non-linearly with the PA6 concentration, suggesting a competition between the reaction pathways leading to their formation.

GPC analyses with RI detector provided the molar mass distribution of the compounds present in the different organic phases (Figure 7).

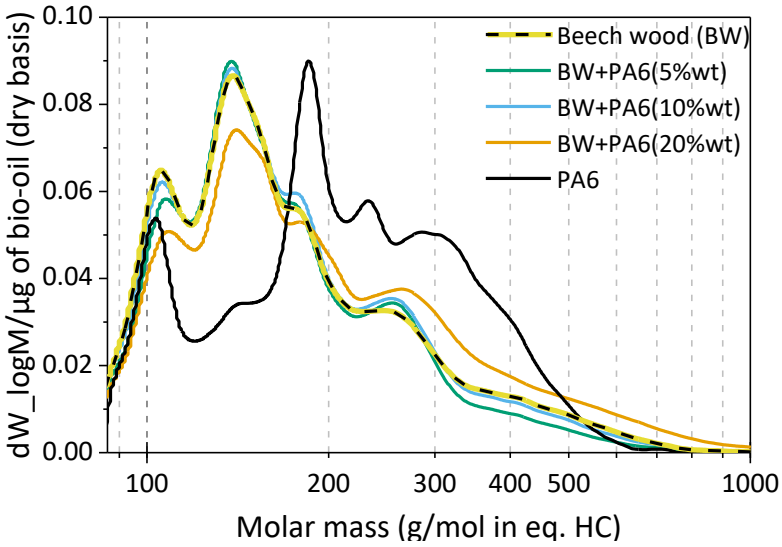

Figure 7 - MW distribution of the organic phase normalized by unit mass of dry bio-oil

At low PA6 concentrations (5 and 10 wt.%), the GPC profiles were very similar to the one obtained with pure BW, with a maximum intensity at ≈140 g/mol, and the MWs below 300 g/mol represented ≈70% of the total area. The organic phase obtained from pure PA6 exhibited a very different profile, with a maximum intensity found at 185 g/mol and the area in the 160-500 g/mol range representing 86% of the total area. With the BW+ 20% PA6 blend, the GPC profile was a combination of the two previous profiles and the formation of heavier compounds was clearly revealed. These modifications are translated in the average molar mass variations reported in Table 3.

Table 3 - Average molar mass of organic fractions

Feedstock	**MW (g/mol, in eq. HC)**
Beech wood	191
BW+5 % PA6	179

BW+ 10% PA6	185
BW+ 20% PA6	219
PA6	228

GPC analyses were also carried out using UV/DAD in order to obtain specific information regarding the unsaturated compounds present in the bio-oils (Figure 8). For comparison, only the results obtained with 100% BW, with BW +20 % PA6 and with 100 % PA6 are shown.

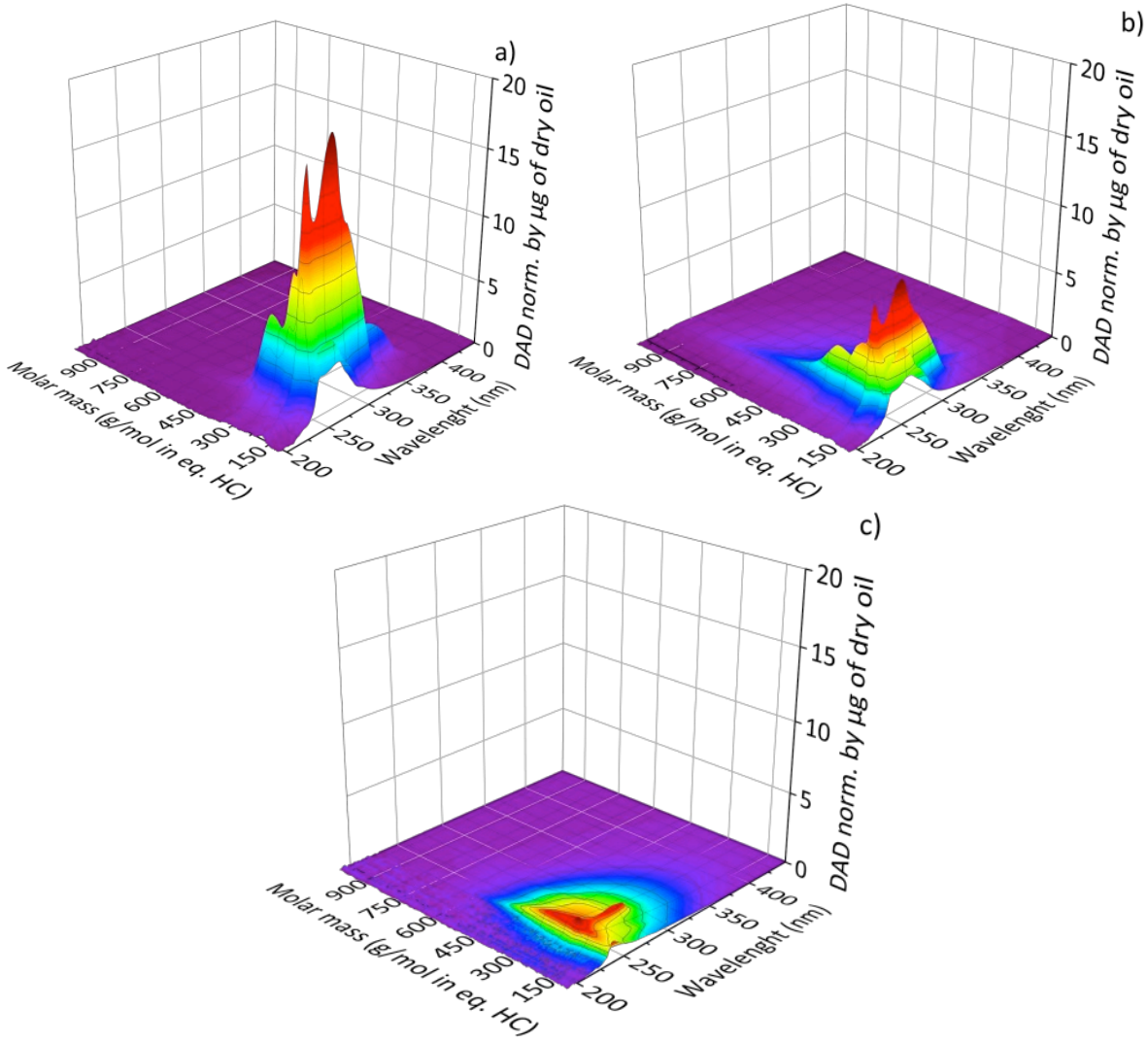

Figure 8 - GPC- DAD chromatograms of organic fraction obtained from (a) BW, (b) BW+ 20% PA6 and (c) PA6

In all cases, the profiles were centered at MWs in the range of 150–200 g/mol and a wavelength close to 267 nm. Absorption in this region is assigned to compounds with conjugated double bond systems such as aromatics, and the peak shifts towards larger wavelengths when the size of the

conjugated system increases (e.g. benzene – peak at 255 nm; naphthalene – 286 nm; anthracene – 375 nm) [16]. The pyrolysis of lignocellulosic biomass produces many aromatic compounds such as guaiacols, syringols, phenols and aromatic ethers. This production was marginal using pure PA6, as evidenced by the intensity close to zero. It was also strongly reduced using the BW+20% PA6 blend, but not proportionally to the concentration of PA6 since the maximum peak intensity decreased by more than 50%.

^{13}C-NMR analyses depicted in Figure 9 show the different functional groups present in the organic phases.

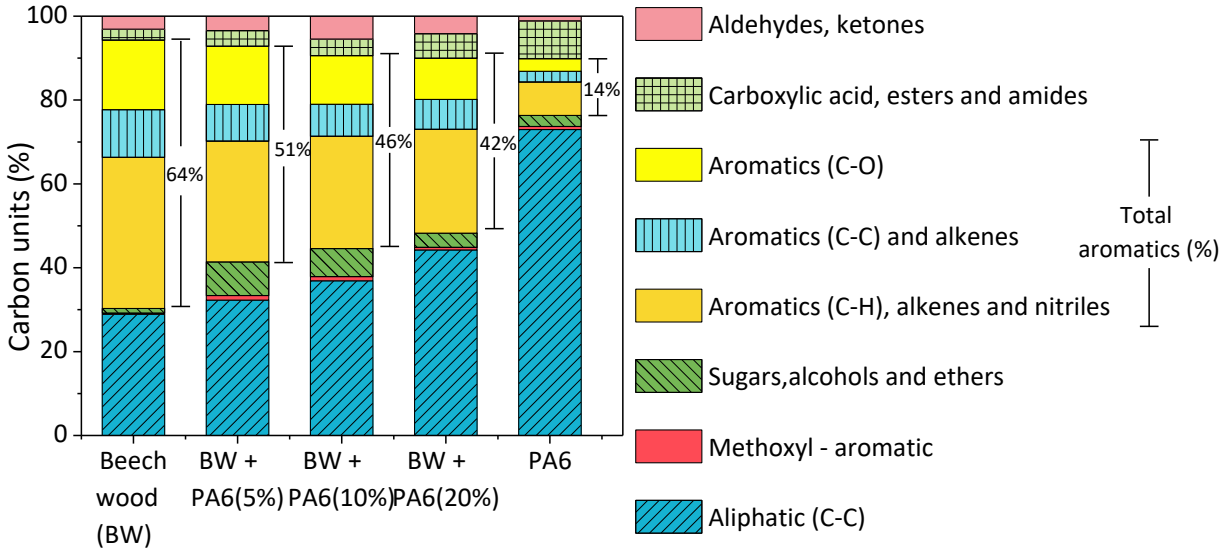

Figure 9 - ^{13}C-NMR - Functional group distribution in the different organic phases

The content of aromatic compounds decreased when the concentration of PA6 increased, in agreement with the GPC-DAD analyses shown previously. It should be mentioned that the chemical shift assigned to nitriles (range 110-130 ppm, e.g.: 5-cyano-1-pentene) is similar to that assigned to aromatic C-H (dark yellow). Therefore, the reduction in aromatic groups was probably underestimated in this analysis. Another case of superposition of chemical shifts is related to the carboxylic acid and amide groups (green with squares): in this case, this concentration growth should be associated mainly to the presence of caprolactam, which was the main degradation product of PA6. Consistently, the amount of aliphatic carbon units increased with the concentration of PA6.

More detailed information about the composition of the organic phases is given by the GC-MS analyses presented in Figure 10.

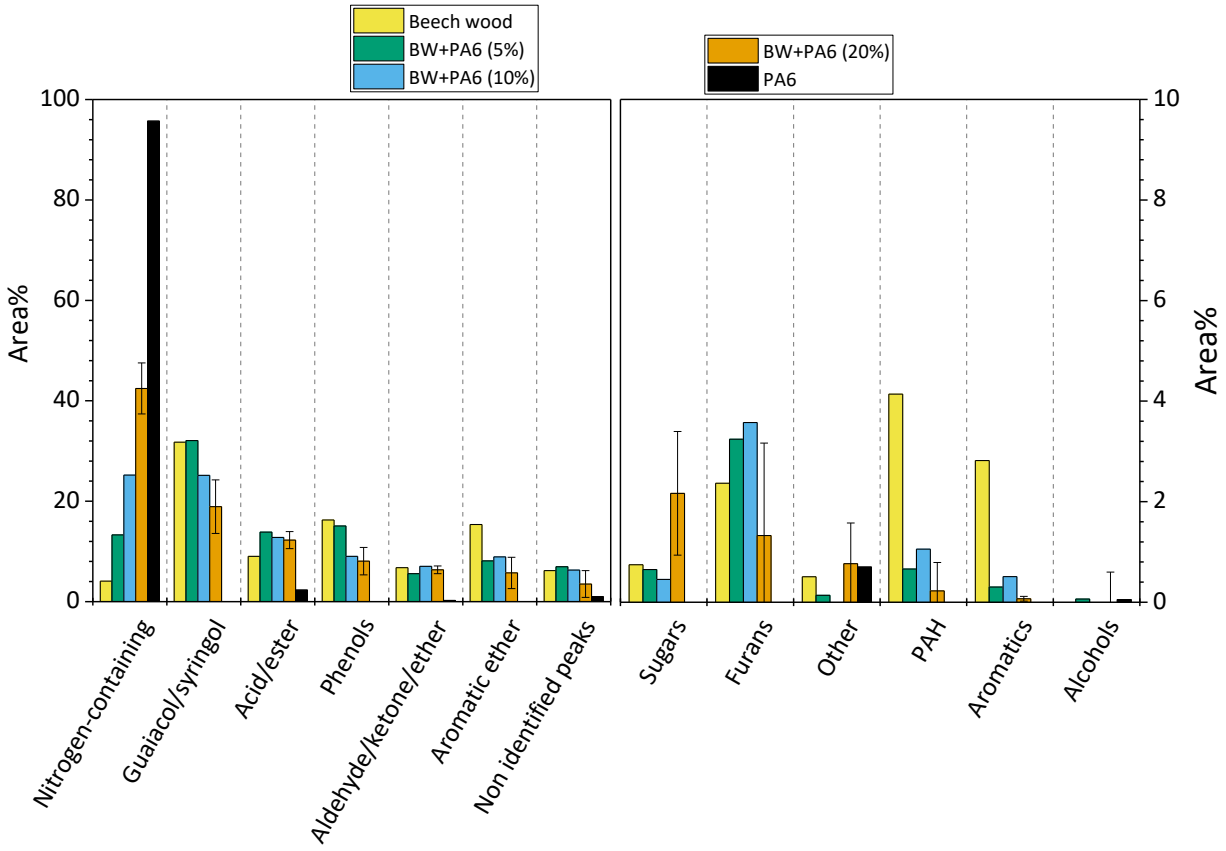

Figure 10 - Relative areas of compounds families identified by GC-MS for the different organic phases

As expected, the concentration of nitrogen-containing compounds grew with the increase in plastic concentration, from 4% with pure beech wood to 96% with pure plastic. Concurrently, there was a progressive reduction in the production of aromatic compounds originating from the biomass, such as guaiacol, syringol and phenols. Moreover, the presence of PA6, even at low concentration (5 wt.%), resulted in a significant drop in the amount of deoxygenated aromatic compounds (i.e. PAH and aromatics). These results confirmed that the catalytic activity was impaired in its oxygen-removal function in the presence of PA6. This was corroborated by the sharp increase in sugar concentration together with a decrease in furans (product of sugars dehydration) when the plastic concentration reached 20 %.

Figure 11 shows the group of compounds obtained with GCxGC-MS analyses.

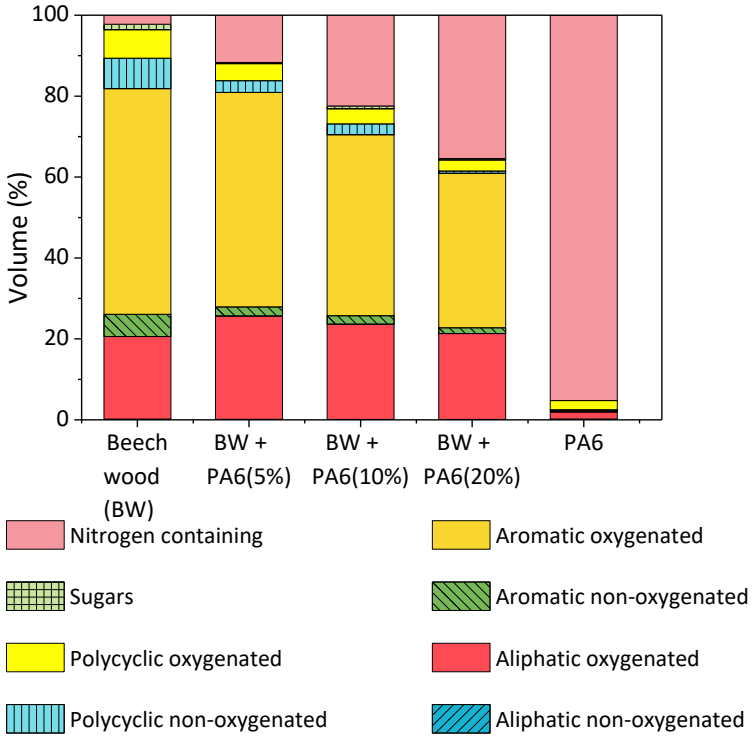

Figure 11 - Relative blob volumes of compound families identified by GCxGC-MS in the organic phases

These results fully support the trends observed with the previous techniques. The selectivity for nitrogen-containing compounds increased proportionally with the concentration of plastic, whereas that for aromatic oxygenated compounds (i.e. guaiacols, syringols, phenols…) decreased. Finally, the groups of fully deoxygenated compounds (non-oxygenated aromatics and polycyclics) were strongly reduced in the presence of plastic. The evolution of peaks assigned to caprolactam and 5-cyano-1-pentene were evidenced in the 3D projections of chromatograms shown in Figure 12.

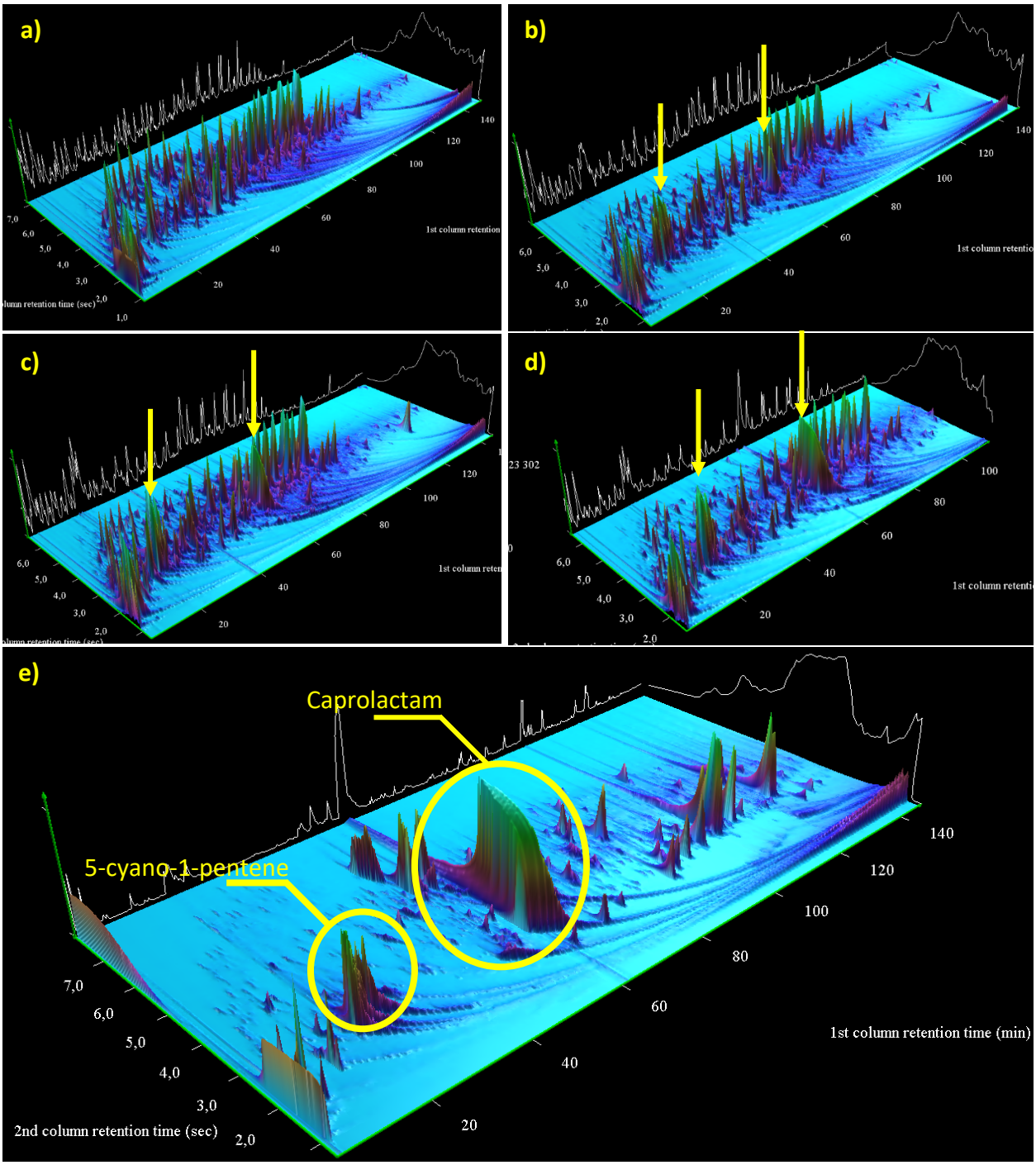

Figure 12 - 3D projections of chromatograms obtained with GCxGC-MS for the organic phases. a) BW; b) BW + PA6 (5%); c) BW + PA6 (10%); d) BW + PA6 (20%); e) PA6.

3.2. Characterization of spent catalysts

The spent catalysts were analyzed to determine the coke composition (CHN) and the amounts of deposited coke were quantified using thermogravimetric analysis (TGA) performed under air to burn the carbon deposits. The results are presented in Figure 13.

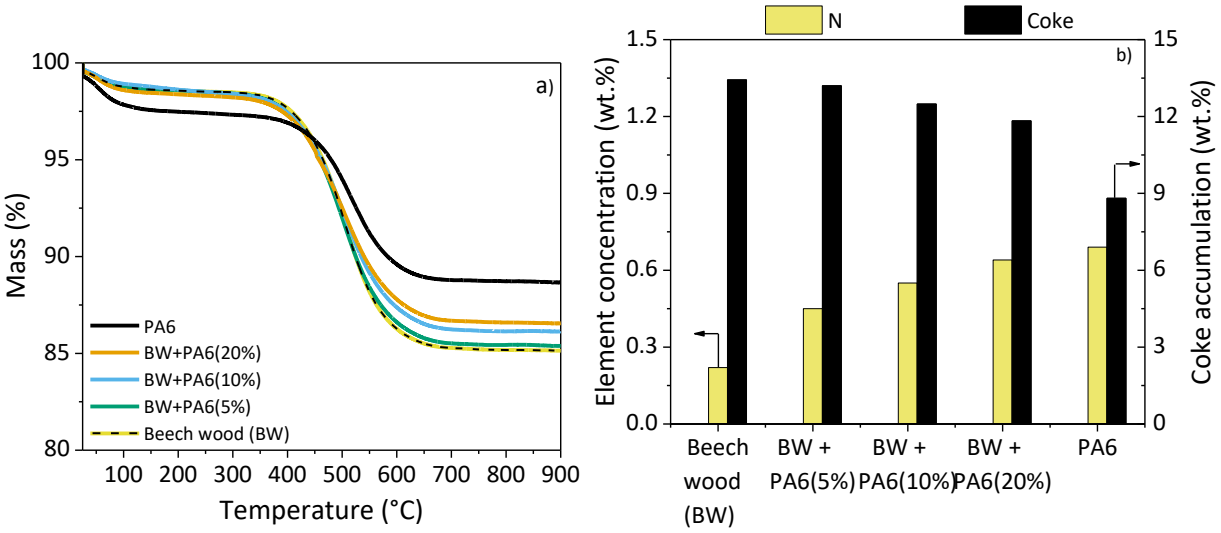

Figure 13 - Mass loss profiles for catalysts after reaction (a); amounts of coke removed from spent catalysts and N content of the coke (b)

For experiments performed in the presence of BW and BW+PA6 blends, an initial mass loss around 1.5 wt.% was observed between 25 and 200°C. It can be attributed to the desorption of water or light compounds adsorbed in the catalyst pores, since the solids were not pre-heated before TGA. The catalyst obtained after the pyrolysis of pure PA6 showed a more significant mass loss in this region (2.5%). This could indicate that N-containing compounds were also adsorbed on the catalytic sites, corroborating the hypothesis of a partial deactivation of HZSM-5. This is also consistent with the increase in liquid products and decrease in gas products with the amount of PA6, shown in Fig. 2, which could indicate a lower cracking activity of the catalyst. The deactivation of acid catalytic sites by nitrogen poisoning is well documented [17–19] and even at low concentration (<0.1%), the presence of N-containing compounds may cause a deactivation of zeolites, as reported by Caeiro et al. [20].

The mass loss between 300 and 900°C was assigned to coke combustion, which took place in a simple one-step profile at similar temperatures, indicating that the carbon deposits were rather

409 homogeneous in their structure. The amount of coke deposited on the catalyst decreased when the
410 PA6 concentration increased; however, the experiment using pure PA6 yielded almost 9 wt.% of
411 coke on the catalyst. The increase in the PA6 amount in the blend also led to a steady rise in the N
412 content in the spent catalyst, although not proportional to PA6 concentration.

413 Several studies reported the beneficial effect of co-pyrolysis with some plastics (notably olefin-
414 derived plastics such as polyethylene and polypropylene) in reducing the catalyst deactivation by
415 coke [6, 17–21]. The explanation relies on the high H content in the plastics that promotes the
416 formation of liquid products, and on the low amounts of aromatic compounds formed during their
417 degradation, which limits the condensation/polymerization reactions of these species. The effect
418 of plastic, however, should be assessed by comparing the effective coke yields with the calculated
419 arithmetic sum of coke yields expected on the basis of a proportional contribution of coke
420 originating from BW and PA6, respectively. This will be described in the next section.

421

422 **3.3. Synergistic effects**

423 The effect of adding PA6 to BW on the pyrolysis products yields and properties has been
424 assessed by comparing the calculated value of each property, based on an arithmetic contribution
425 of the values obtained using pure BW and pure PA6 (in wt. %), with the value of this property
426 effectively measured, using the following equation [26]:

427 $$Y_{estimated(BW+\alpha PA-6)} = \alpha Y_{exp(BW)} + (1-\alpha) Y_{exp(PA6)} \quad (1)$$

428 where $Y_{exp(BW)}$ is the experimental value of the parameter evaluated (e.g. phase selectivity, N
429 concentration, coke content…) obtained with pure BW, $Y_{exp(PA6)}$ is the experimental value
430 obtained with pure PA6 and α is the concentration of plastic in the blend.

431 The synergistic impact (ΔY) was evaluated using the following equation [27]:

432 $$\Delta Y = \frac{Y_{exp(BW+\alpha PA6)} - Y_{estimated(BW+\alpha PA6)}}{Y_{estimated(BW+\alpha PA6)}} \times 100\% \quad (2)$$

433 where $Y_{exp(BW+\alpha PA6)}$ is the experimental value obtained from the co-pyrolysis of feedstock
434 containing α% of plastic and $Y_{estimated(BW+\alpha PA6)}$ was calculated using Eq.(1). The evaluation of
435 the synergistic impact for different parameters of the pyrolysis process is presented in Table 4.

436

437 Table 4 - Synergistic impact between BW and PA6 for different parameters

Parameter	Experimental			Calculated	ΔY
	100% BW	BW+20%PA6	100% PA6	BW+20%PA6	
Gas products (%)	22	16	2	18	-11%
Liquid products (%)	57	64	70	60	+8%
Solid products (%)	20	19	29	22	-14%
Coke on catalyst (wt.%)	13.43	11.83	8.81	12.50	-5%
N (wt.%) in organic phase	0.5	6.1	14.3	3.3	+87%
H/C organic phase	1.1	1.3	1.6	1.2	+6%
O/C organic phase	0.24	0.16	0.01	0.19	-19%

438

439 The co-pyrolysis of PA6 and BW resulted in a gas phase selectivity below what was expected.
440 According to the literature [24, 25], the melting temperature of PA6 is between 170°C and 260°C.
441 At the inlet of the heated zone, the plastic starts to melt and it may partially cover the wood
442 particles, which could hinder the evolution of gaseous products from the wood. Besides, it can
443 modify the heat conductivity of wood chips and delay the evolution of gases [4].

444 Conversely, the production of liquid products benefited from a positive synergistic effect, with
445 the experimental selectivity for condensable products higher than the calculated value. The blend
446 of BW with PA6 chips could have prevented the premature agglomeration of the melted polymer,
447 as observed in the experiment with pure PA6, and which interferes with heat transfer and with the
448 cracking of the polymeric chain. Another evidence of this agglomeration was provided by the
449 aspect and consistency of the chars obtained after pyrolysis: using pure BW, the char consisted of
450 blackened but well separated wood particles, while the chars obtained from co-pyrolysis of
451 BW+PA6 blends consisted of aggregated particles, with a certain mechanical resistance. The same
452 phenomenon also explains the synergy effect on the solid product selectivity, BW contributing to
453 improve the cracking of PA6, which led to lesser amounts of solid products.

The nitrogen content in the organic phase also exhibited a strong positive synergistic effect, with an experimental value 85% higher than the calculated value. This could be due to the promotion of PA6 cracking by water, present at high concentration, and by oxygen-containing radicals originating from the biomass, which could attack the polymer chain [30].

The impact of PA6 on the H/C atomic ratio of bio-oils was modest (+6%). In contrast, the BW+20 wt.% PA6 blend showed a synergistic effect of -19% on the O/C atomic ratio of the organic phase, indicating that the overall deoxygenation was improved in the presence of PA6, although fewer totally deoxygenated compounds were formed, as shown previously. During the initial stages of co-pyrolysis, the degradation of biomass released highly reactive oxygen-containing species. These species may attack the polymer, subtracting hydrogen from its structure and favoring the chain scission, as mentioned before. In return, this hydrogen transfer from the polymer contributed to the stabilization of the biomass-derived compounds, reducing the coke formation through polymerization and condensation reactions [27, 28]. This effect on coke formation was confirmed by the synergistic impact that showed a coke deposition 5% lower than the calculated value.

The reactions leading to deoxygenation (dehydration, decarbonylation, decarboxylation) occur mainly inside the zeolite pores and, as regards HZSM-5 (pore diameter – 0.55 nm), many compounds were too large to be able to enter the pores. For example, levoglucosan first needs to be converted into furan, by dehydration on acid sites of the external catalyst surface, which can then diffuse into the pores to complete the deoxygenation [33]. Therefore, coke deposition at the entrance or inside the pores reduces the deoxygenation activity. As co-pyrolysis with PA6 decreased the rate of coke deposition, the deoxygenation activity was maintained for a longer period, contributing to the reduction in the O/C ratio.

4. Conclusion

The co-pyrolysis of beech wood (BW) and polyamide-6 (PA6) combined with *ex situ* catalytic treatment of the pyrolysis vapors was investigated at different BW/PA6 ratios. The presence of PA6 resulted in a decrease in the gaseous product selectivity and in the coke deposition on the catalyst. N-containing compounds derived from PA6 were found in the liquid phase (mainly as caprolactam) and in the solid products, but no N-containing gaseous product was formed. The

production of aromatic compounds derived from the wood was also reduced in the presence of PA6.

This work showed that the properties of the co-pyrolysis products were not the simple arithmetic addition of the properties of the products obtained by pyrolysis of pure BW or pure PA6: positive or negative synergistic effects were observed depending on the property considered. The most important synergistic effect was observed on the concentration of nitrogen in the organic phase (+87 %). It was attributed to a higher depolymerization of PA6 promoted by reactive oxygenated species originating from the wood, and probably associated to the negative synergistic effects observed on coke deposition (-5 %) and on the O/C ratio (-19 %) of the co-pyrolysis oil.

ACKNOWLEDGEMENTS

This project has received funding from the European Union's Horizon 2020 research and innovation programme under grant agreement N° 818120 (Waste2Road ). The authors also thank Véronique Bounor-Légaré (CNRS and University of Lyon) for providing different samples of plastics.

References

[1] W. de Rezende Locatel, C. Mohabeer, D. Laurenti, Y. Schuurman, N. Guilhaume, Co-pyrolysis of beech wood and polyamide-6: Effect of HZSM-5 catalyst on the properties of pyrolysis oils, Journal of Analytical and Applied Pyrolysis. (2022) 105696. https://doi.org/10.1016/j.jaap.2022.105696.

[2] X. Zhang, H. Lei, S. Chen, J. Wu, Catalytic co-pyrolysis of lignocellulosic biomass with polymers: a critical review, Green Chemistry. 18 (2016) 4145–4169. https://doi.org/10.1039/C6GC00911E.

[3] Y.-T. Cheng, G.W. Huber, Production of targeted aromatics by using Diels–Alder classes of reactions with furans and olefins over ZSM-5, Green Chem. 14 (2012) 3114. https://doi.org/10.1039/c2gc35767d.

[4] X. Liu, K.G. Burra, Z. Wang, J. Li, D. Che, A.K. Gupta, On deconvolution for understanding synergistic effects in co-pyrolysis of pinewood and polypropylene, Applied Energy. 279 (2020) 115811. https://doi.org/10.1016/j.apenergy.2020.115811.

[5] X. Li, J. Li, G. Zhou, Y. Feng, Y. Wang, G. Yu, S. Deng, J. Huang, B. Wang, Enhancing the production of renewable petrochemicals by co-feeding of biomass with plastics in catalytic fast pyrolysis with ZSM-5 zeolites, Applied Catalysis A: General. 481 (2014) 173–182. https://doi.org/10.1016/j.apcata.2014.05.015.

[6] P. Ghorbannezhad, S. Park, J.A. Onwudili, Co-pyrolysis of biomass and plastic waste over zeolite- and sodium-based catalysts for enhanced yields of hydrocarbon products, Waste Management. 102 (2020) 909–918. https://doi.org/10.1016/j.wasman.2019.12.006.

[7] L.S. Diaz-Silvarrey, A. McMahon, A.N. Phan, Benzoic acid recovery via waste poly(ethylene terephthalate) (PET) catalytic pyrolysis using sulphated zirconia catalyst, Journal of Analytical and Applied Pyrolysis. 134 (2018) 621–631. https://doi.org/10.1016/j.jaap.2018.08.014.

[8] C. Areeprasert, J. Asingsamanunt, S. Srisawat, J. Kaharn, B. Inseemeesak, P. Phasee, C. Khaobang, W. Siwakosit, C. Chiemchaisri, Municipal Plastic Waste Composition Study at Transfer Station of Bangkok and Possibility of its Energy Recovery by Pyrolysis, Energy Procedia. 107 (2017) 222–226. https://doi.org/10.1016/j.egypro.2016.12.132.

[9] A.L. Patrício Silva, J.C. Prata, A.C. Duarte, D. Barcelò, T. Rocha-Santos, An urgent call to think globally and act locally on landfill disposable plastics under and after covid-19 pandemic: Pollution prevention and technological (Bio) remediation solutions, Chemical Engineering Journal. 426 (2021) 131201. https://doi.org/10.1016/j.cej.2021.131201.

[10] W. de Rezende Locatel, D. Laurenti, Y. Schuurman, N. Guilhaume, Can Paints and Varnish Impair the Physicochemical Properties of Wood Pyrolysis Oils?, Energy Fuels. 35 (2021) 17739–17754. https://doi.org/10.1021/acs.energyfuels.1c02568.

[11] W. de Rezende Locatel, D. Laurenti, Y. Schuurman, N. Guilhaume, Ex-situ catalytic

upgrading of pyrolysis vapors using mixed metal oxides, Journal of Analytical and Applied Pyrolysis. 158 (2021) 105241. https://doi.org/10.1016/j.jaap.2021.105241.

[12] S.A. Channiwala, P.P. Parikh, A unified correlation for estimating HHV of solid, liquid and gaseous fuels, Fuel. 81 (2002) 1051–1063. https://doi.org/10.1016/S0016-2361(01)00131-4.

[13] B. Omais, M. Courtiade, N. Charon, D. Thiébaut, A. Quignard, M.-C. Hennion, Investigating comprehensive two-dimensional gas chromatography conditions to optimize the separation of oxygenated compounds in a direct coal liquefaction middle distillate, Journal of Chromatography A. 1218 (2011) 3233–3240. https://doi.org/10.1016/j.chroma.2010.12.049.

[14] W.B. Fisher, L. Crescentini, Caprolactam, in: John Wiley & Sons Inc (Ed.), Kirk-Othmer Encyclopedia of Chemical Technology, John Wiley & Sons, Inc., Hoboken, NJ, USA, 2015: pp. 1–11. https://doi.org/10.1002/0471238961.0301161806091908.a01.pub2.

[15] K.B. Ansari, S.Z. Hassan, R. Bhoi, E. Ahmad, Co-pyrolysis of biomass and plastic wastes: A review on reactants synergy, catalyst impact, process parameter, hydrocarbon fuel potential, COVID-19, Journal of Environmental Chemical Engineering. 9 (2021) 106436. https://doi.org/10.1016/j.jece.2021.106436.

[16] UV talk latter - vol. 2, Shimadzu, n.d. https://www.shimadzu.com/an/sites/shimadzu.com.an/files/pim/pim_document_file/journal/talk_letters/13197/jpa112002.pdf.

[17] A. de Lucas, P. Cañizares, A. Durán, Improving deactivation behaviour of HZSM-5 catalysts, Applied Catalysis A: General. 206 (2001) 87–93. https://doi.org/10.1016/S0926-860X(00)00586-X.

[18] T. Takahashi, M.N.A. Nasution, T. Kai, Effects of acid strength and micro pore size on ε-caprolactam selectivity and catalyst deactivation in vapor phase Beckmann rearrangement over acid solid catalysts, Applied Catalysis A: General. 210 (2001) 339–344. https://doi.org/10.1016/S0926-860X(00)00828-0.

[19] R. Van Grieken, J.M. Escola, J. Moreno, R. Rodríguez, Nitrogen and sulphur poisoning in alkene oligomerization over mesostructured aluminosilicates (Al-MTS, Al-MCM-41) and nanocrystalline n-HZM-5, Applied Catalysis A: General. 337 (2008) 173–183. https://doi.org/10.1016/j.apcata.2007.12.011.

[20] G. Caeiro, J. Lopes, P. Magnoux, P. Ayrault, F. Ramoaribeiro, A FT-IR study of deactivation phenomena during methylcyclohexane transformation on H-USY zeolites: Nitrogen poisoning, coke formation, and acidity–activity correlations, Journal of Catalysis. 249 (2007) 234–243. https://doi.org/10.1016/j.jcat.2007.04.005.

[21] Y.-M. Kim, J. Jae, B.-S. Kim, Y. Hong, S.-C. Jung, Y.-K. Park, Catalytic co-pyrolysis of torrefied yellow poplar and high-density polyethylene using microporous HZSM-5 and mesoporous Al-MCM-41 catalysts, Energy Conversion and Management. 149 (2017) 966–973. https://doi.org/10.1016/j.enconman.2017.04.033.

[22] C. Dorado, C.A. Mullen, A.A. Boateng, H-ZSM5 Catalyzed Co-Pyrolysis of Biomass and Plastics, ACS Sustainable Chemistry & Engineering. 2 (2014) 301–311. https://doi.org/10.1021/sc400354g.

[23] H. Zhang, J. Nie, R. Xiao, B. Jin, C. Dong, G. Xiao, Catalytic Co-pyrolysis of Biomass and Different Plastics (Polyethylene, Polypropylene, and Polystyrene) To Improve Hydrocarbon Yield in a Fluidized-Bed Reactor, Energy Fuels. 28 (2014) 1940–1947. https://doi.org/10.1021/ef4019299.

[24] M. Alam, D. Rammohan, N.R. Peela, Catalytic co-pyrolysis of wet-torrefied bamboo sawdust and plastic over the zeolite H-ZSM-5: Synergistic effects and kinetics, Renewable Energy. 178 (2021) 608–619. https://doi.org/10.1016/j.renene.2021.06.109.

[25] Y. Xue, A. Kelkar, X. Bai, Catalytic co-pyrolysis of biomass and polyethylene in a tandem micropyrolyzer, Fuel. 166 (2016) 227–236. https://doi.org/10.1016/j.fuel.2015.10.125.

[26] Z. Wang, K.G. Burra, T. Lei, A.K. Gupta, Co-pyrolysis of waste plastic and solid biomass for synergistic production of biofuels and chemicals-A review, Progress in Energy and Combustion Science. 84 (2021) 100899. https://doi.org/10.1016/j.pecs.2020.100899.

[27] P. Lu, Q. Huang, A.C. (Thanos) Bourtsalas, Y. Chi, J. Yan, Synergistic effects on char and oil produced by the co-pyrolysis of pine wood, polyethylene and polyvinyl chloride, Fuel. 230 (2018) 359–367. https://doi.org/10.1016/j.fuel.2018.05.072.

[28] H. Bockhorn, A. Hornung, U. Hornung, J. Weichmann, Kinetic study on the non-catalysed and catalysed degradation of polyamide 6 with isothermal and dynamic methods, Thermochimica Acta. 337 (1999) 97–110. https://doi.org/10.1016/S0040-6031(99)00151-3.

[29] D. Bhattacharyya, P. Maitrot, S. Fakirov, Polyamide 6 single polymer composites, Express Polymer Letters. 3 (2009) 525–532. https://doi.org/10.3144/expresspolymlett.2009.65.

[30] X. Liu, K.R.G. Burra, Z. Wang, J. Li, D. Che, A.K. Gupta, Towards enhanced understanding of synergistic effects in co-pyrolysis of pinewood and polycarbonate, Applied Energy. 289 (2021) 116662. https://doi.org/10.1016/j.apenergy.2021.116662.

[31] X. Zhang, H. Lei, L. Zhu, M. Qian, X. Zhu, J. Wu, S. Chen, Enhancement of jet fuel range alkanes from co-feeding of lignocellulosic biomass with plastics via tandem catalytic conversions, Applied Energy. 173 (2016) 418–430. https://doi.org/10.1016/j.apenergy.2016.04.071.

[32] M.H.M. Ahmed, N. Batalha, H.M.D. Mahmudul, G. Perkins, M. Konarova, A review on advanced catalytic co-pyrolysis of biomass and hydrogen-rich feedstock: Insights into synergistic effect, catalyst development and reaction mechanism, Bioresource Technology. 310 (2020) 123457. https://doi.org/10.1016/j.biortech.2020.123457.

[33] K. Praveen Kumar, S. Srinivas, Catalytic Co-pyrolysis of Biomass and Plastics (Polypropylene and Polystyrene) Using Spent FCC Catalyst, Energy Fuels. 34 (2020) 460–473. https://doi.org/10.1021/acs.energyfuels.9b03135.

610